Draft version November 14, 2018
Typeset using LaTeX default style in AASTeX62

High- and Low-α Disk Stars Separate Dynamically at all Ages

Suroor S Gandhi[1] and Melissa K Ness[2,3]

[1]*Department of Physics, New York University, 726 Broadway, New York, NY, 10003, USA*
[2]*Center for Computational Astrophysics, Flatiron Institute, 162 5th Ave., New York, NY 10010, USA*
[3]*Department of Astronomy, Columbia University, 550 W 120th St, New York, NY 10027, USA*

ABSTRACT

Context: There is a dichotomy in the Milky Way in the [α/Fe] v. [Fe/H] plane, in which stars fall into (a) high-α, and (b) low-α enhancement. The high-α sequence primarily comprises old stars, and the low-α sequence primarily has young stars. The origin of this dichotomy is poorly understood.
Aims: We use orbital properties calculated from Gaia DR2 measurements to characterize the correlation between dynamics and chemical enrichment, as a function of age. Specifically, we examine if the high- and low-α sequences are dynamically distinct at all ages, or if age sets the orbital properties of stars irrespective of their α-enhancement.
Data and Method: We use ages for 58,278 stars, measured to a precision of 40%, from the LAMOST survey and we calculate orbital actions from proper motions and parallaxes given by Gaia's DR2. We use orbital actions J_R, J_z, and J_ϕ (or L_z) as labels of stellar dynamics.
Results: We find that *at all ages*, the high- and low-α sequences are dynamically distinct. We also find a population of old low-α stars which might be part of a past merger with the Milky Way.
Conclusion: The high- and low-α sequences are linked to discrete formation and evolutionary processes.

Keywords: keywords here

1. INTRODUCTION

As more and more extensive surveys like GALAH (De Silva et al. 2015), LAMOST (Cui et al. 2012; Luo et al. 2016), APOGEE (Majewski et al. 2017), RAVE (Kunder et al. 2017; Casey et al. 2017), and Gaia (Gilmore et al. 2012; Gaia Collaboration et al. 2018) catalog larger regions in and around our Galaxy, understanding the structure and formation of the Milky Way is within our reach more than it has ever been before. Comprehending the structure of the Milky Way is the most accessible way to understand galactic evolution in our universe. Each part of the Milky Way (the bulge, disk, and halo) has stars which have different chemical and dynamical properties, as well as possibly different birth properties. Deducing the formation histories of various parts of the Milky Way by studying the chemistry, kinematics, age, etc of stars in different regions can lead us to understand epochs in the life of the galaxy itself (Silva Aguirre et al. 2018). The disk of the Milky Way is the most expansive part where most of the stellar mass resides, and potentially holds immense information which can shed light on how the universe evolves on galactic as well as cosmological scales.

Research continues to support the hypothesis that disk stars in the Milky Way which have been observed so far fall into two broad categories of chemical composition: (1) α-enhanced or high-α stars, and (2) α-poor or low-α stars (Fuhrmann 1998; Gratton et al. 2000; Prochaska et al. 2000; Bensby et al. 2003; Venn et al. 2004; Bensby et al. 2005; Adibekyan et al. 2011; Bensby et al. 2014; Anders et al. 2014; Nidever et al. 2014; Hayden et al. 2015). The bimodality is often inferred to be the signature of two distinct populations (Mackereth et al. 2018). Spectroscopic surveys have enabled scientists to establish correlations between α-enhancement and properties such as age (Wyse & Gilmore 1988; Haywood et al. 2013; Bensby et al. 2014; Bergemann et al. 2014): high-α stars are mostly old, and low-α stars are typically young. Low-α stars range over several dex of $[Fe/H]$ but tend to have a lower ratio of α elements to iron-peak elements. Quite possibly, the distinct formation timescales and velocity dispersion of the "thin"

Corresponding author: Suroor S Gandhi
ssg487@nyu.edu

and "thick" components of the Milky Way disk could translate into α-abundance signatures. However, the correlation between α-enhancement of stars and their location in the thin or thick disk is contested because significant mixing between the two α-sequences has become apparent in recent work (Feltzing & Bensby 2008; Schönrich & Binney 2009; Adibekyan et al. 2011; Loebman et al. 2011; Bensby et al. 2014; Silva Aguirre et al. 2018; Bland-Hawthorn et al. 2018). Despite the lack of a clear distinction between the two α-sequences as far as position within the Galaxy is concerned, the discovery of other properties which are distinct lead to the hypothesis that their birth and evolution tracks might be separable in some way.

To make any sort of generalizable statement about how the two α-sequences separate, we need access to accurately measured properties for a large sample of stars. Gaia DR2 (Gaia Collaboration et al. 2018) measured positions, distances, and proper motions for ∼1.3 billion objects in the sky which makes it possible to study the dynamics of stars with unprecedented accuracy. The Large sky Area Multi-Object Spectroscopic Telescope (LAMOST) Survey (Cui et al. 2012) is one of the most extensive catalogs of low-resolution (R∼ 1800) spectroscopic data at present. It is an optical ($3650 - 9000$Å) survey, and its second data release (Luo et al. 2016) covered $\sim 500,000$ red giants. *The Cannon*, developed by Ness et al. (2015), provides a data-driven method to infer information about a large number of stars by channeling and combining data from across various astronomical surveys. It has been a challenge to accurately measure ages of stars because age can usually only be inferred from visible properties, such as chemical abundance from spectra (Rix & Bovy 2013; Bovy et al. 2016; Ho et al. 2017). However, using *The Cannon*, Ho et al. (2017) created the largest catalog of age estimates for $\sim 230,000$ red giants by inferring the masses from $[C/M]$ and $[N/M]$ abundances. Therefore, now we have access to dynamics and ages of a larger sample than ever before.

Actions provide a powerful description of stellar dynamics because they can encapsulate information to uniquely define an orbit (Trick et al. 2018). We use cylindrical coordinates (r, ϕ, z) for positions of stars and calculate actions using:

$$J_i \equiv \oint_{orbit} p_i dx_i$$

where $i = r, \phi, z$, and p_i is the conjugate momentum (Beane et al. 2018). If we approximate the Milky Way's potential to be axisymmetric and it's evolution over time to be slow enough, actions are constants of motion for timescales of the order of several orbits (Bland-Hawthorn et al. 2018). The three actions, J_r, J_ϕ (or angular momentum, L_z), and J_z separately provide physical interpretations of a star's orbit. (We will use L_z instead of J_ϕ in our discussion hereafter.) J_r indicates the eccentricity of an orbit, or an orbit's deviation from a circle. L_z is a direct indicator of the radius of the orbit, and J_z indicates the maximum vertical distance of an orbit from the galactic plane.

2. DATA

We investigate $\sim 60,000$ red giant stars in the disk ($<= 2$ *kpc* from the Sun) taken from the LAMOST Survey and use their ages as calculated by Ho et al. (2017) (precise up to 0.2 dex), as well as the proper motion and parallax information acquired from Gaia DR2.

Fig. 1a shows the $[\alpha/M]$ vs $[Fe/H]$ plane colored by age. We see that, as expected, there are two collections of stars that emerge clearly in this plane (separated roughly by the black line). These two groups are the high-α or α-rich sequence (above the black line), and the low-α or α-poor sequence (below the black line). The high-α stars in our sample are ∼7,000 in number and have a high ratio of α elements (Ne, Mg, Si, S, Ar, etc) to iron-peak elements, but low iron content (i.e., low $[Fe/H]$). The low-α stars ($\sim 51,000$ in number) span several decades of metallicity, and have lower content of α elements. At a metallicity of ∼ -0.2, there is a "knee" in the plot (Fig. 1a) after which the disparity in the amount of α elements and iron-peak elements goes down, and the high-α and low-α sequences appear to converge (Hayden et al. 2015).

Fig. 1b shows the age distribution of our sample of (disk) stars. It becomes clear that the mean ages of the two sequences are pretty distinct, in the sense that high-α stars are typically older than the low-α population. This trend is also indicated by the age coloring in Fig. 1a.

Fig.s 1c,d show the spatial extent of $\sim 150,000$ stars which include disk stars from beyond 2 *kpc*, and halo stars, all of which we have age information for. This "super-sample" extends from a galactic radius of ~ 6 *kpc* to ~ 14 *kpc*, and ~ 2 *kpc* above and below the galactic plane. However, our conclusions about dynamical distinction in the high- and low-α sequences are restricted to disk stars within a distance of 2 *kpc* of the Sun. This distance cut was implemented because we have used inverse parallax as a proxy for distance, and that estimate becomes erroneous at large distances as shown by **?**. The spatial extent of stars that we take into account for our study are within the dashed circles in

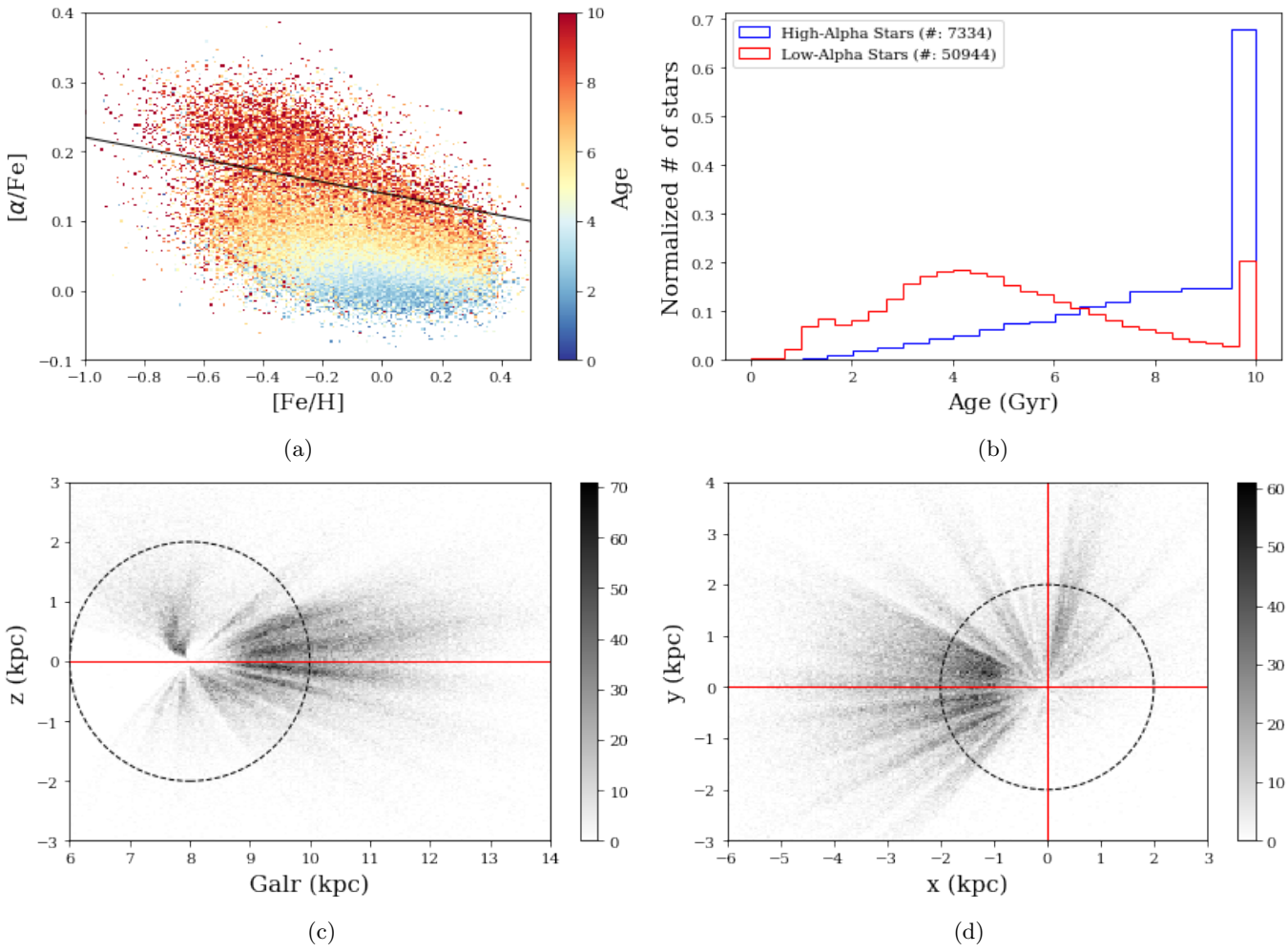

Figure 1. This figure shows the main properties of our data sample of the LAMOST disk red giants. (a) $\sim 60,000$ stars in the $[\alpha/Fe]$ v. $[Fe/H]$ plane, colored by age. A black line is drawn approximately through where the dichotomy between the two α-enrichment sequences occurs. We can see that high-α stars (above the black line) are mostly old ($>\sim 8$ Gyr), whereas the low-α stars (below the line) are typically much younger. (b) The normalized age distribution for $\sim 7,000$ high-α stars (in blue), and $\sim 51,000$ low-α stars (in red). These histograms also show that the two α sequences have different mean ages. (c) The spatial spread of the $\sim 150,000$ strong sample is shown in a density plot of z v. galactic radius (in kpc). The galactic plane at $z = 0$ is shown by the horizontal red line. Our analyses are restricted to stars within $2kpc$ of the Sun, which is demarcated by the dashed circle. (d) The x v. y distribution is shown in a density plot, and the disk stars that we study are, again, within the dashed circle of radius 2 kpc. The intersection of the two red lines marks the position of the Sun.

fig.s 1c,d, and these disk stars comprise our main sample. Out of a total of 58,537 stars, there are 7,527 high-α stars and 51,010 low-α stars in our sample.

In Fig.2, the top panel shows normalized distributions of the galactocentric radius, R, for the high- and low-α sequences, and the lower panel shows the spread of the distance from the galactic plane, z, for different metallicities. Histograms with varying line thickness represent different metallicity ranges. We see a gradient in the radii of low-α stars as metallicity changes, as expected from prior literature which has proposed that the metallicity gradient in the Milky Way comes about largely from low-α stars (**?**).

Our sample has the following cuts as Ho et al. (2017) (§5) which had enabled them to calculate ages for the stars accurate to 0.2 dex:

$$-0.8 < [Fe/H] < 0.25$$
$$4000 < T_{eff} < 5000$$
$$1.8 < log(g) < 3.3$$

$$-0.05 < [\alpha/Fe] < 0.3$$

the lower limit on $[\alpha/Fe]$ above (0.05) doesn't seem consistent with fig. 1a? Double checked with Anna's paper

Additionally, in order to have precise actions, we need accurate distance measurements (Coronado et al. 2018; Trick et al. 2018; Beane et al. 2018). We use the inverse of parallax ($1/\omega$) as a proxy for distance and restrict our sample to stars which have a parallax error ($\delta\omega/\omega$) of less than 20%.

We calculate actions using the same method as Trick et al. (2018): by first converting the observable positions and velocities into cartesian (X, Y, Z) and heliocentric (U_{HC}, V_{HC}, W_{HC}) coordinates, and finally to galactocentric $(R, \phi, z, v_R, v_T, v_z)$ coordinates using the `galpy` package (Bovy 2015). U is the velocity component towards the galactic center, V is the component in the direction of rotation of the galaxy, and W is the component towards the galactic north pole. The coordinate conversion from cartesian and heliocentric to galactocentric is necessary to calculate the actions J_R, J_z, and L_z in `galpy` and is done using $(U_\odot, V_\odot, W_\odot) = (11.1, 12.24, 7.25)$ $km\ s^{-1}$ as the sun's velocity in the Local Standard of Rest (LSR) (Schönrich et al. 2010) and $(R_\odot, \phi_\odot, z_\odot) = (8, 0, 0.025)$ (with $R_\odot, z_\odot$ in kpc) as the sun's position within the galaxy (Jurić et al. 2008).

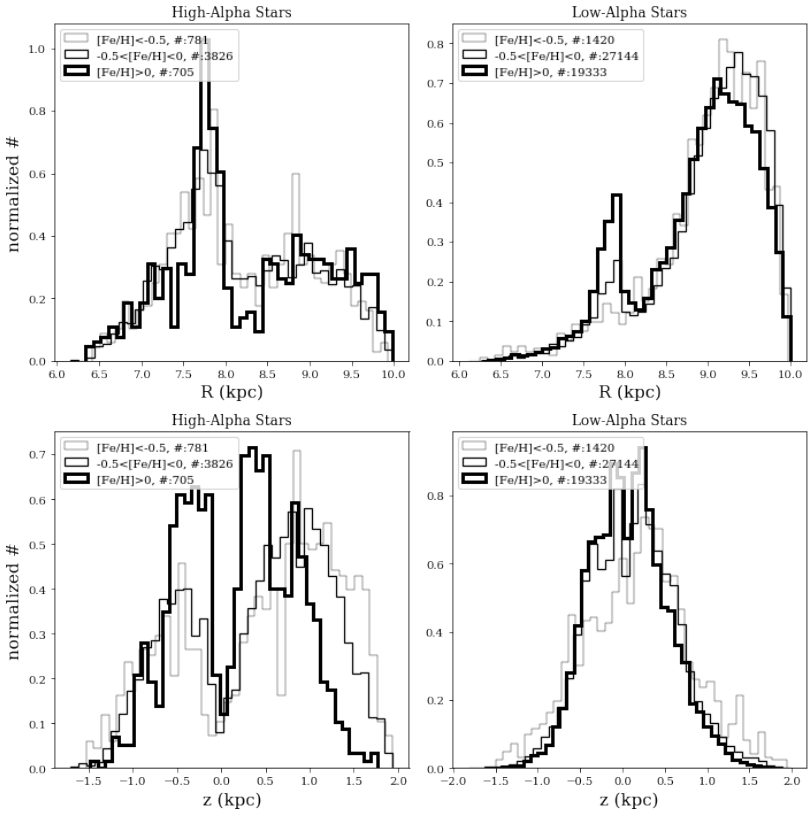

Figure 2. Normalized histograms for R (top panel) and z (lower panel) for the two α-sequences (high-α to the left, low-α to the right) in three different metallicity bins. The numbers of stars for each metallicity bin and α sequence is recorded in the legends. We see in the top panel that the two α sequences have quite distinguishable mean radii for all metallicity ranges. In the lower panel, the distinction between mean z is not that clear perhaps because of the $<= 2$ kpc restriction on distance.

3. RESULTS

3.1. *The actions as a function of age*

When we examine the actions J_R, J_z and L_z for the two sequences as a function of stellar age for 7,334 high-α stars, and 50,944 low-α stars. We find that the high- and low-α stars have very distinct mean dynamical properties. Fig. 3 shows the running mean of each of the actions as a function of age for the two α sequences (high-α in blue, low-α in

red). It is important to note from these plots that each α sequence displays distinct dynamical behavior in all three orbital parameters: eccentricity (J_R), height above the galactic plane (J_z), and radius (L_z). Moreover, the distinction in dynamical trends of the high- and low-α stars is present consistently at all ages.

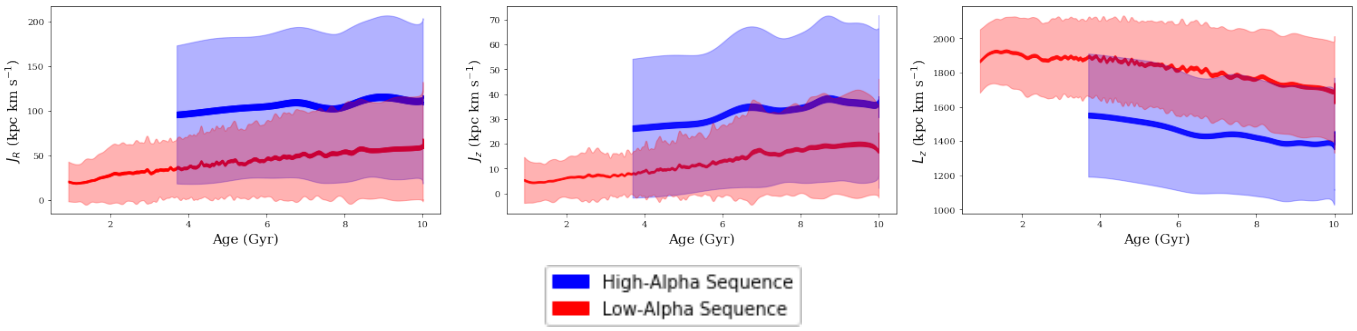

Figure 3. The main results of our work are shown in these three plots. They strongly indicate that high- and low-α sequences display distinct dynamical trends at all ages. The running means of each of the three actions for 7,334 high-α stars and 50,944 low-α stars are plotted against age. The high- and the low-α sequences are represented by the solid blue curve and the solid red curve respectively. The running means have been smoothed with a Gaussian filter using $\sigma = 200$. The thickness of the solid curves represents the standard error, and the colored shaded regions are the respective standard deviation in actions.

The running means of actions and age were calculated using a bin size of 300 stars for both the α-sequences. The 1σ standard deviation is used to estimate the dispersion in the running means, and the standard errors are found by simply dividing the standard deviations by the bin size. In table 1 we report the ratio of average dispersion to average action for each of the three actions of the two α sequences. Admittedly, the numbers reported are very rough, and they do not take into account the change in variance over time seen in J_R and J_z of low-α sequence. However, they do give an adequate idea of the spread of our sample.

Action	mean var/mean action	
	high-α	low-α
J_R	0.79	0.98
J_z	0.9	1.13
L_z	0.24	0.13

Table 1. A table showing the ratio of average variance to average of the running mean of each action for the two α sequences. The variances and running means used in this table are those which are shown in fig. 3.

There is a difference of almost a factor of 2 between the running means of J_R and J_z for the high-α and low-α stars, whereas the low-α stars on average have ~ 1.25 times the angular momentum (L_z) compared to high-α stars.
Although there are slight gradients in the means with respect to age, since these gradients might be affected by the selection function of the LAMOST survey, a quantitative claim cannot be made as of yet about the trend in dynamics with respect to age.

3.2. *High- and Low-α Sequence Actions as a Function of Metallicity*

We analyze the two α-sequences in various ways to look for more properties that might distinguish them from each other, and correlate chemistry with dynamics and location within the Galaxy. Fig. 4 shows smoothed running means of J_R, J_z, and L_z versus age for high-α stars in the left panel, and the low-α stars in the right panel, for three different metallicity ranges. The varied thickness of line corresponds to a different $[Fe/H]$ bin. The standard errors on these curves are on the order of the thickness of the lines. From these plots, it is quite clear that the mean eccentricity, divergence from the galactic plane, and radial location of the two α-sequences is significantly distinct even if they have the same metallicity, which might further support our findings that dynamics are correlated with α-enrichment.

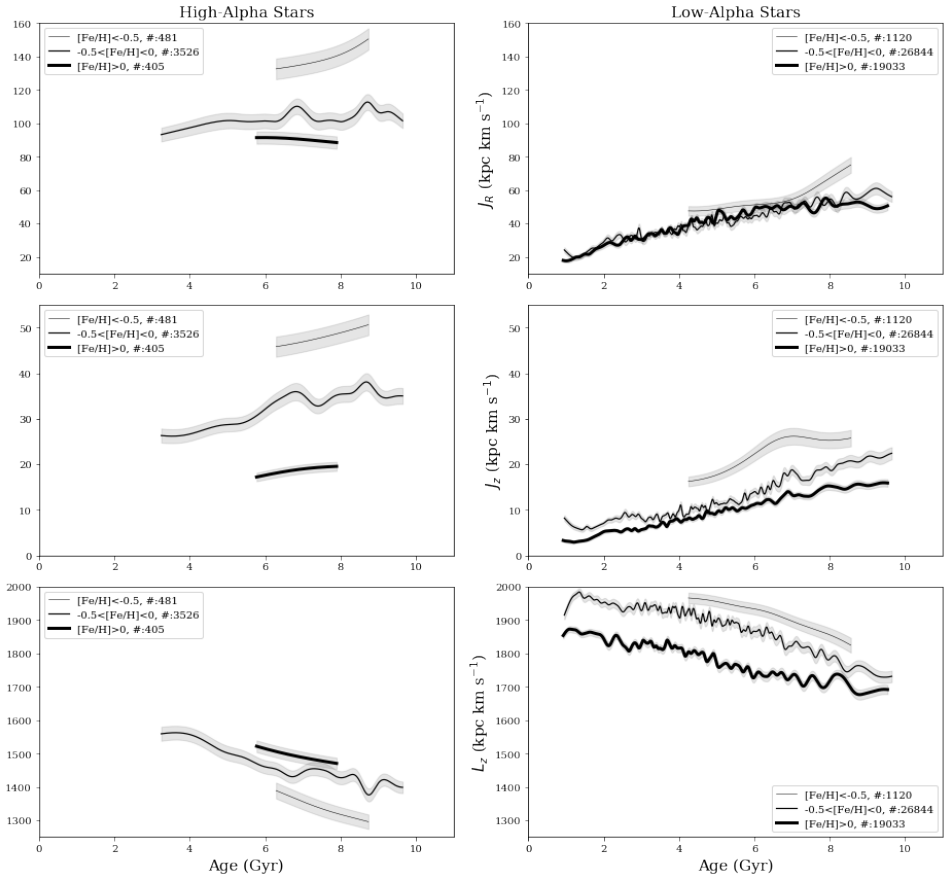

Figure 4. This figure shows smoothed running means of J_R, J_z, and L_z as a function of age in three different metallicity bins. Each $[Feh/H]$ bin is represented by a different line thickness. The high-α stars are plotted in the left panel, and the low-α stars in the right panel. We used $\sigma = 100$ for smoothening the data. The standard errors are shown by the light gray shaded regions around each curve, which we can see are on the order of the thickness of the lines. The number of stars for each α sequence and metallicity bin is recorded in the legends. These plots make it clear that the two α sequences have quite distinct dynamical properties (associated with each of the three actions) regardless of metallicity.

3.3. *High and low alpha sequence as a function of spatial selection, z*

Separating the α-sequences according to their height from the galactic plane helps decouple their dynamics from their location in the Milky Way. We find that at the same distance from the galactic plane (within the disk), the two sequences have mean actions that are different from each other at all ages, as shown in fig. 5. The standard errors on all curves (not shown in this figure) are on the order of the thickness of the lines.

3.4. *Bayesian ages*

We also used ages and actions from a catalog developed by Sanders & Das (2018) to check whether we get similar results with their data. In their analysis, Sanders & Das employed Bayesian neural networks to date stars, and the Gaia DR2 data to find the actions using the Stackel fudge method. Fig.6 shows the plots obtained using the data from Sanders & Das (2018), similar to our results in fig. 3. These plots have 30,579 high-α stars, and 122,668 low-α stars. These stars are also within 2 *kpc* of the Sun, and we did a quality cut such that parallax error is $< 20\%$. That these data also indicate a distinction in dynamical trends between the two α-sequences is quite encouraging.

4. DISCUSSION

4.1. *Orbital properties of the High- and Low-α Sequences*

Studying the actions J_R, J_z, and L_z as a function of age for the two α-sequences makes it clear that disk stars in the solar neighborhood that fall into different α-enrichment groups have very different mean orbital properties at *all* ages.

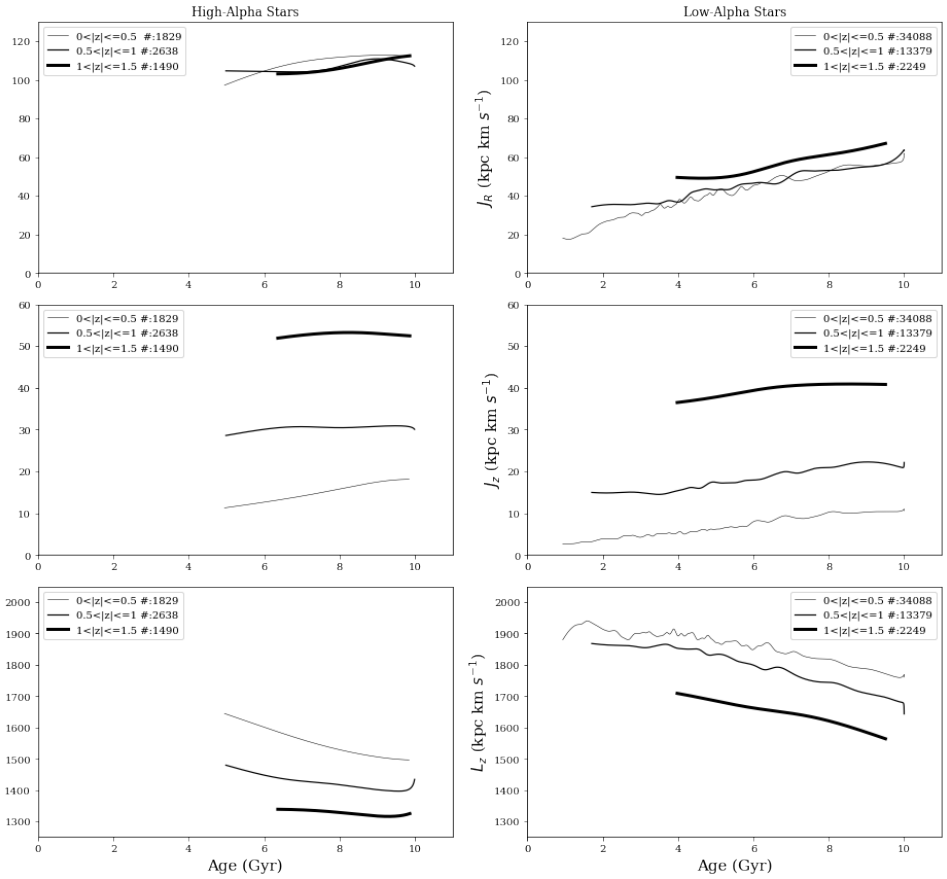

Figure 5. This figure shows smoothed running means of J_R, J_z, and L_z v. age for the high- (left panel) and low-α (right panel) sequences separated into bins of height above the galactic plane, $|z|$. The thickness of the lines is proportional to the height above the plane. $\sigma = 300$ was used for smoothening the data. Division into $|z|$ bins helps decouple the $|z|$-positions of the stars from their chemistry and dynamics as we can see that even at the same height from the plane, the two α-sequences have different J_R, J_z, and L_z, i.e., different dynamical properties, at all ages. Standard errors have been left out in these plots because they are on the order of the thickness of the curves.

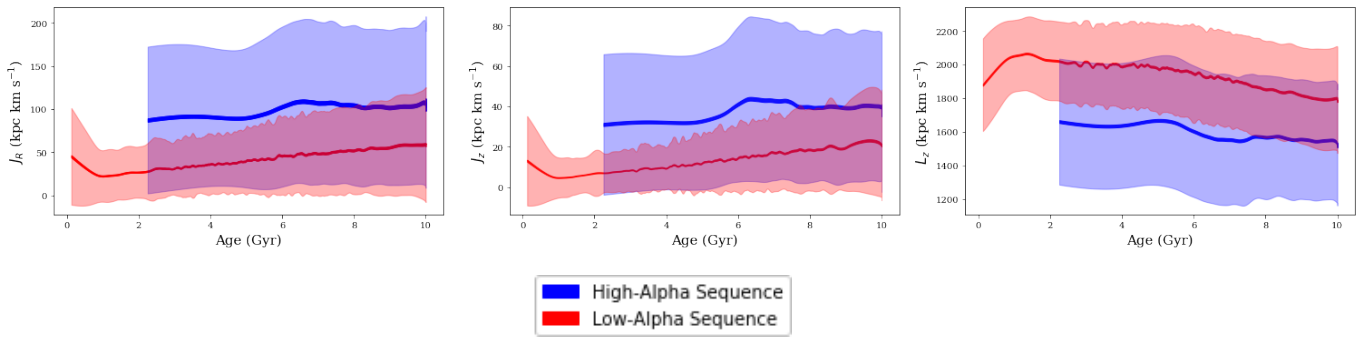

Figure 6. The running means of each of the three actions (from Sanders&Das (2018)) for 30,579 high-α stars and 122,668 low-α stars are plotted against age. The high- and the low-α sequences are represented by the solid blue curve and the solid red curve respectively. The running means have been smoothed with a Gaussian filter using $\sigma = 200$. The thickness of the solid curves represents the standard error, and the colored shaded regions are the respective standard deviation in actions. These plots quite closely match fig. 3.

The fact that this dichotomy in the action plane is present throughout all ages, for all actions, is a strong indication that high- and low-α sequences form distinct populations which have different evolution and birth properties. Fig. 3

shows our main results, and from this figure we can understand what the nature of the orbits of stars in the high- or low-α sequence is, at least with respect to each other. Orbits of high-α stars are on average more eccentric (have greater J_R) than the low-α stars, almost consistently by a factor of two. We see a similar relationship between the two sequences in how much their orbits diverge from the galactic plane (or J_z): the high-α sequence has orbits which go almost up to twice the height from the plane compared to low-α stars. The angular momentum (L_z) of low-α stars is ~ 1.25 times that of the high-α stars, which indicates that low-α stars on average have larger radii than high-α stars. This is consistent with the idea that low-α stars are present in regions farther from the galactic center than the high-α stars (Beane et al. 2018; Hayden et al. 2015).

It is interesting to note that we find a valley between two slight peaks (in fig. 3) in J_R and J_z for the high-α sequence between age $\sim 6-9$ Gyr, and a slight peak between two valleys in L_z for high-α stars in the same age window. We see similar signatures in analyzing LAMOST stars from Sanders & Das (2018), as can be seen in fig. 6. The presence of a perturbation in J_z was also suggested by Beane et al. (2018) (§3.2) for stars in the APOKASC2 sample (independent of α-enrichment).

The fact that there is a detectable perturbation seen in all three actions for our data sample could be a strong indication of a merger event with the Milky Way, which altered the dynamical properties of stars. We anticipate that the merger was one which triggered formation of new stars (e.g., a gas cloud merger), as opposed to a merger with a star cluster which brought in pre-existing stars. Had the merging object been a star cluster, it would have kicked the orbits of Milky Way stars of all ages, resulting in a sort of step in the actions in fig. 3 after ~ 6 Gyr, and not peaks localized in age. A gas cloud merger, on the other hand, would trigger formation of stars with J_R, J_z, and L_z distinct from other pre-existing stars in the neighborhood, and the newly formed stars would all have approximately one age.

Further corroborating this hypothesis is the fact that these "bumps" are localized in α-enrichment as well as metallicity, because the gas cloud would have a consistent average chemical composition. As can be seen in fig. 4, they appear only in the high-α sequence in the range of $-0.5 < [Fe/H] < 0$, within the same age range ($\sim 6-9$ Gyr). This leads us to predict that in future work, it might be found that the general elemental composition of this possibly foreign population of high-α stars which are $\sim 6-9$ Gyr old is different from the other high-α stars in the Galaxy.

4.2. *Infall (An Appended Discussion)*

As discussed earlier, Haywood et al. (2013); Bensby et al. (2014); Bergemann et al. (2014) corroborate the correlation between chemical composition and stellar age, according to which most high-α stars are old and most low-α stars are young. There is also a distinction between the two α-sequences according to where within the disk they lie: the high-α sequence is believed to reside in the thick disk, whereas the low-α sequence is mostly in the thin disk of the galaxy (Haywood et al. 2013).

We investigate the subpopulation of low-α stars at relatively low metallicity ($[Fe/H] \sim -0.6$) which happen to be atypically older than the rest of the low-α sequence.

we currently don't have a figure showing this population of old low-α stars

However, for this analysis, we include stars beyond the disk, as well as halo stars. These stars can be examined fairly carefully since we have access to their dynamical properties, as well as their ages.

Following Gaia DR2, a spurt of research has found strong indications of prior mergers with the Milky Way (Myeong et al. 2018; Koppelman et al. 2018; Helmi et al. 2018). In particular, Helmi et al. (2018) find a retrograde population in the halo near the Sun which they call the "Gaia Enceladus" and show that it might have merged with the Milky Way ~ 10 Gyr ago. The specific old low-α subpopulation that we see in our sample also appears in the group of stars that Helmi et al. (2018) study. At $[Fe/H] \sim -0.6$, the Gaia Enceladus is shown to consist of stars which are $\sim 10-13$ Gyr old and α-poor compared to the typical thick disk stars (Helmi et al. 2018). Thus, Helmi et al. (2018) conclude that these stars must belong to a population which has a lower star formation rate and hence a different birth and evolution history from the thick disk.

The fact that the old, low-α stars seen by Helmi et al. (2018) belong in the halo implies that their orbits must be highly eccentric for them to be observed in the solar neighborhood, and thus J_R for these stars must be higher on average, and their average radii (or L_z) can be expected to be less than the majority of stars in our sample. To confirm whether the subpopulation of old, low-α stars that we see coincides with the stars in Gaia Enceladus, we examine the dynamics of the low-α sequence by plotting L_z vs J_R colored by age. The L_z vs J_R plane in Fig.7 separates the disk and halo stars in the following way: stars with a wide range of eccentricity (J_R) and angular momenta (L_z) represent the disk, whereas low angular momentum and high eccentricity are indicative of halo orbits. The figure clarifies that

the old low-α stars in our sample do indeed lie near the halo. Therefore, it is highly probable that this atypical subpopulation of old low-α stars in our sample can at least partially be explained by the Gaia Enceladus.

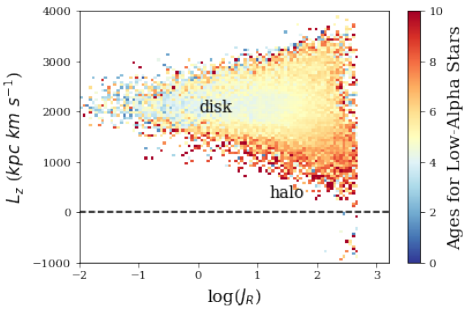

Figure 7. A 2D histogram of $\sim 130,000$ disk and halo low-α stars in the L_z v. $log(J_R)$ plane, colored by age. The L_z v. $log(J_R)$ plane visually separates the disk and the halo; stellar orbits with a variety of angular momenta (L_z) and eccentricity (J_R) values represent the disk and result in the triangular shape of the distribution, whereas the tapering bottom end of the distribution with low L_z and high J_R characterizes the halo orbits. We can see that a lot of the old low-α stars appear near the halo.

4.3. *Orbital properties of Infall*

- Is this old potential infall described in Helmi et al., 2018 distinct in any way in action space from the rest of the stars? If not, is this because it is phase mixed?

5. CONCLUSION

We calculated actions (J_R, J_z, and L_z) using dynamical information from Gaia DR2 , and used ages for LAMOST red giants (in the disk near the Sun) from Ho et al. (2017). We have found clear indications that α-enrichment is correlated with dynamical properties of stellar orbits. Our main conclusions are summarized below:

1. Consistently throughout all ages, the high- and low-α sequences exhibit distinct mean trends in eccentricity (J_R), divergence from galactic plane(J_z), and angular momentum (L_z)—the three dynamical properties which (simplistically, but uniquely) characterize a stellar orbit. This result can be seen clearly in fig. 3. This implies that the two α sequences are distinct populations in the Milky Way, with different birth and evolution properties.

2. The conclusion that chemistry is strongly linked to orbital properties of stars at all ages has been shown to be independent of metallicity (fig. 4) as well as z (fig. 5).

3. We find two subpopulations of stars which differ from the other stars in their neighborhood:

   a . High-α stars with actions which are noticeably distinct from other stars at certain ages ($\sim 6-9$ Gyr) can be seen in fig. 3 and fig. 6, and

   b . Low-α stars which are atypically older and live predominantly in the halo

   We suggest that these two subpopulations might be indications of merger events in the Milky Way: (a) being a merger with a gas cloud, and (b) a merger with Gaia Enceladus (Helmi et al. 2018).

- conclude by linking to other papers e.g. Duong 2018, Victor Silva Aguirre 2018, Beane 2018, Hayden 2018.

6. ACKNOWLEDGEMENTS

We would like to thank...

REFERENCES

Adibekyan, V. Z., Santos, N. C., Sousa, S. G., & Israelian, G. 2011, A&A, 535, L11

Anders, F., Chiappini, C., Santiago, B. X., et al. 2014, A&A, 564, A115

Beane, A., Ness, M., & Bedell, M. 2018, ArXiv e-prints, arXiv:1807.05986
Bensby, T., Feltzing, S., & Lundström, I. 2003, A&A, 410, 527
Bensby, T., Feltzing, S., Lundström, I., & Ilyin, I. 2005, A&A, 433, 185
Bensby, T., Feltzing, S., & Oey, M. S. 2014, A&A, 562, A71
Bergemann, M., Ruchti, G. R., Serenelli, A., et al. 2014, A&A, 565, A89
Bland-Hawthorn, J., Sharma, S., Tepper-Garcia, T., et al. 2018, ArXiv e-prints, arXiv:1809.02658
Bovy, J. 2015, ApJS, 216, 29
Bovy, J., Rix, H.-W., Schlafly, E. F., et al. 2016, ApJ, 823, 30
Casey, A. R., Hawkins, K., Hogg, D. W., et al. 2017, ApJ, 840, 59
Coronado, J., Rix, H.-W., & Trick, W. H. 2018, ArXiv e-prints, arXiv:1804.07760
Cui, X.-Q., Zhao, Y.-H., Chu, Y.-Q., et al. 2012, Research in Astronomy and Astrophysics, 12, 1197
De Silva, G. M., Freeman, K. C., Bland-Hawthorn, J., et al. 2015, MNRAS, 449, 2604
Feltzing, S., & Bensby, T. 2008, Physica Scripta Volume T, 133, 014031
Fuhrmann, K. 1998, A&A, 338, 161
Gaia Collaboration, Brown, A. G. A., Vallenari, A., et al. 2018, A&A, 616, A1
Gilmore, G., Randich, S., Asplund, M., et al. 2012, The Messenger, 147, 25
Gratton, R. G., Carretta, E., Matteucci, F., & Sneden, C. 2000, A&A, 358, 671
Hayden, M. R., Bovy, J., Holtzman, J. A., et al. 2015, ApJ, 808, 132
Haywood, M., Di Matteo, P., Lehnert, M. D., Katz, D., & Gómez, A. 2013, A&A, 560, A109
Helmi, A., Babusiaux, C., Koppelman, H. H., et al. 2018, ArXiv e-prints, arXiv:1806.06038
Ho, A. Y. Q., Rix, H.-W., Ness, M. K., et al. 2017, ApJ, 841, 40
Jurić, M., Ivezić, Ž., Brooks, A., et al. 2008, ApJ, 673, 864
Koppelman, H., Helmi, A., & Veljanoski, J. 2018, ApJL, 860, L11
Kunder, A., Kordopatis, G., Steinmetz, M., et al. 2017, AJ, 153, 75
Loebman, S. R., Roškar, R., Debattista, V. P., et al. 2011, ApJ, 737, 8
Luo, A.-L., Zhao, Y.-H., Zhao, G., et al. 2016, VizieR Online Data Catalog, 5149
Mackereth, J. T., Crain, R. A., Schiavon, R. P., et al. 2018, MNRAS, 477, 5072
Majewski, S. R., Schiavon, R. P., Frinchaboy, P. M., et al. 2017, AJ, 154, 94
Myeong, G. C., Evans, N. W., Belokurov, V., Sanders, J. L., & Koposov, S. E. 2018, ApJL, 856, L26
Ness, M., Hogg, D. W., Rix, H.-W., Ho, A. Y. Q., & Zasowski, G. 2015, ApJ, 808, 16
Nidever, D. L., Bovy, J., Bird, J. C., et al. 2014, ApJ, 796, 38
Prochaska, J. X., Naumov, S. O., Carney, B. W., McWilliam, A., & Wolfe, A. M. 2000, AJ, 120, 2513
Rix, H.-W., & Bovy, J. 2013, A&A Rv, 21, 61
Sanders, J. L., & Das, P. 2018, MNRAS, 481, 4093
Schönrich, R., & Binney, J. 2009, MNRAS, 399, 1145
Schönrich, R., Binney, J., & Dehnen, W. 2010, MNRAS, 403, 1829
Silva Aguirre, V., Bojsen-Hansen, M., Slumstrup, D., et al. 2018, MNRAS, 475, 5487
Trick, W. H., Coronado, J., & Rix, H.-W. 2018, ArXiv e-prints, arXiv:1805.03653
Venn, K. A., Irwin, M., Shetrone, M. D., et al. 2004, AJ, 128, 1177
Wyse, R. F. G., & Gilmore, G. 1988, AJ, 95, 1404